To measure qualitatively the effectiveness of the proposed control approach in reducing impact velocities, the performance of the proposed control strategy has been compared to those obtained by controlling the valve only via a sequence of proper levels of currents designed via a trial and error approach. We note that the impact velocities have been computed offline by fitting linearly the position of the armature around a small neighbor of each impact time. In doing so, unavoidable delays, introduced when filters are used to reconstruct the velocity, do not affect the impact velocity measurements.

Our analysis have shown that, with an open-loop control, about 85% of the considered impact velocities are in the range of 0.2–0.8 m/s with a mean value of 0.5 m/s. Such values are unacceptable for automotive applications in terms of the noise produced by the device. Moreover, a high value of the mean impact velocity can strongly reduce the lifespan of the valve and even cause system failures.

Much better results, instead, can be achieved if the feedback decoupling control approach is used. In particular, by means of the proposed control approach, the mean value of the impact velocity is less than 0.1 m/s; hence, it is reduced to about five times with respect to the open-loop method with the benefit of the lifespan of the component and noise reduction. Moreover, more than 55% of the impact velocity occurrences are less than 0.1 m/s and they never excess the 0.5 m/s.

VII. Conclusion

A detailed mathematical model of an electromechanical valve actuator for camless engines has been validated on different sets of experimental data. It has been proven that the strongly nonlinear dynamics of the device are well captured by the model during fundamental valve maneuvers. To show the effectiveness and the usefulness of the model for control purposes, a model-based decoupling control scheme (presented in the literature only theoretically) has been furthermore implemented and experimentally tested to tackle the valve seating control problem with clear benefits in the reduction of impact velocities.

References

[1] V. Picron, Y. Postel, E. Nicot, and D. Durrieu, "Electro-magnetic valve actuation system: First steps toward mass production," SAE Tech. Paper 2008-01-1360, 2008.

[2] A. di Gaeta, U. Montanaro, S. Massimino, and C. I. Hoyos-Velasco, "Experimental investigation of a double magnet EMVA at key-on engine: A mechanical resonance based control strategy," *SAE Int. J. Engines*, vol. 3, pp. 352–372, 2010.

[3] P. Mercorelli, "An antisaturating adaptive preaction and a slide surface to achieve soft landing control for electromagnetic actuators," *IEEE/ASME Trans. Mechatronics*, vol. 17, no. 1, pp. 76–85, Feb. 2012.

[4] J. Tsai, C. R. Koch, and M. Saif, "Cycle adaptive feedforward approach controllers for an electromagnetic valve actuator," *IEEE Trans. Control Syst. Technol.*, vol. 20, no. 3, pp. 738–746, May 2012.

[5] L. Liu and S. Chang, "Improvement of valve seating performance of engine's electromagnetic valvetrain," *Mechatronics*, vol. 21, no. 7, pp. 1234–1238, Oct. 2011.

[6] A. di Gaeta, V. Giglio, and G. Police, "Model-based decoupling control of a magnet engine valve actuator," *SAE Int. J. Engines*, vol. 2, no. 2, pp. 254–271, Apr. 2010.

[7] A. di Gaeta, L. Glielmo, V. Giglio, and G. Police, "Modeling of an electromechanical engine valve actuator based on a hybrid analytical-FEM approach," *IEEE/ASME Trans. Mechatronics*, vol. 13, no. 6, pp. 625–637, Dec. 2008.

[8] M. di Bernardo, A. di Gaeta, C. I. Hoyos Velasco, and S. Santini, "Energy-based key-on control of a double magnet electromechanical valve actuator," *IEEE Trans. Control Syst. Technol.*, [Online]. Available: http://ieeexplore.ieee.org, doi: 10.1109/TCST.2011.2162332

Dynamic Displacement Sensing, System Identification, and Control of a Speaker-Based Tendon Vibrator via Accelerometers

Ozkan Celik, Hunter B. Gilbert, and Marcia K. O'Malley

***Abstract*—In this paper, we develop a speaker-based tendon vibrator capable of applying vibrations with sustained amplitudes and desired time–frequency profiles to be used in inducing kinesthetic illusions. For modeling and control of the tendon vibrator, we propose and experimentally validate a method for real-time dynamic displacement sensing based on accelerometers. We tested the accuracy of displacement measurements by comparing the movements of the vibrator measured with differential accelerometers to those measured by a high resolution optical encoder. We completed frequency domain system identification of the vibrator and obtained a parametric transfer function model via displacements sensed by the encoder and by analog and digital integration. We show that within the frequency range of interest 20 –100 Hz, analog and digital integration methods were successful in capturing an accurate model of the vibrator. Under feedforward control, developed tendon vibrator is able to generate sustained 2-mm peak-to-peak vibrations throughout the frequency range of interest.**

***Index Terms*—Accelerometer-based displacement sensing, accelerometers, artificial proprioception, double integrator, frequency domain system identification, kinesthetic illusions, tendon vibrator.**

I. Introduction

Despite the significant advancements in functionality and complexity of prosthetic devices, novel and intuitive sensory feedback mechanisms for prosthetics are yet to be developed. Controlled kinesthetic illusions via tendon vibration may constitute one potential method for implementing artificial proprioception for prosthetics.

Vibration of muscle tendons around 80–100 Hz [1], [2] has been shown to induce realistic movement illusions at various joints of the human body [3]. Recently, Roll *et al.* [1] showed that it is possible to induce illusions of specific movement trajectories, such as traces of numbers or letters, by designing the vibration frequency profiles within 20–100 Hz, based on mimicking the Ia muscle spindle afferent discharge response profiles during actual movements along the corresponding trajectories.

Tendon vibrators used in the mentioned studies control only the frequency and not the amplitude (displacement) of vibrations. Lack of displacement control leads to decreased vibration amplitudes at higher frequencies, as is apparent in [4], and may constitute the reason behind subharmonic discharge rates of muscle spindle primary endings at higher end of the frequency range observed in [5]. The uncontrolled variation of vibration amplitude with frequency potentially impedes accurate control of illusory movement trajectories.

Manuscript received November 12, 2010; revised July 26, 2011; accepted March 27, 2012. Date of publication May 8, 2012; date of current version January 10, 2013. Recommended by Technical Editor N. Chaillet.

O. Celik was with the Department of Mechanical Engineering and Materials Science, Rice University, Houston, TX. He is now with the School of Engineering, San Francisco State University, San Francisco, CA (e-mail: ocelik@sfsu.edu).

H. B. Gilbert was with the Department of Mechanical Engineering and Materials Science, Rice University, Houston, TX. He is now with the Department of Mechanical Engineering, Vanderbilt University, Nashville, TN (e-mail: hunter.b.gilbert@vanderbilt.edu).

M. K. O'Malley is with the Department of Mechanical Engineering and Materials Science, Rice University, Houston, TX (e-mail: omalleym@rice.edu).

Color versions of one or more of the figures in this paper are available online at http://ieeexplore.ieee.org.

Digital Object Identifier 10.1109/TMECH.2012.2195326

Our goal in this study is to develop a cost-effective tendon vibrator with displacement control, to be used in experimental protocols on evaluating and improving controllability and consistency of tendon vibration-induced movement illusions. More specifically, the design specification for the tendon vibrator is the capability to generate vibrations with sustained amplitude of 2-mm peak-to-peak throughout the frequency range 20–100 Hz. In order to satisfy this specification, we used a speaker as the actuator and developed a method for displacement sensing based on double integration of differential acceleration.

Sensing of displacement using only inertial measurement devices (IMDs) such as rate gyros and accelerometers is an active research topic with many diverse applications in biomechanics [6], [7], [8], human motion tracking [9], [10] and robotics [11], [12]. The main challenge in using integration to obtain velocity or position data from IMDs is direct current (dc) drift in measurements [6]. Even very small dc offsets in acceleration measurements lead to significant errors that increase linearly in single integration and parabolically in double integration. This severely complicates the problem of sensing static (dc) displacements using IMDs. A significant amount of literature has focused on improving absolute displacement estimations in spite of dc offsets.

One common method to minimize effects of drift in displacement estimation has been fusion of acceleration, velocity, and sometimes direction of gravity data via a Kalman filter algorithm [10]. A more commonly used method to avoid drifts is strapdown integration, or resetting of the integration results at specified intervals [6], [8], [13]. More recently, an interesting approach that allowed determining body angular velocities without integration was reported by Parsa *et al.* [11]. These studies show that long-term and reliable absolute displacement sensing based on only acceleration measurements is not currently achievable. Avoiding drift while sensing static displacements in real time requires either more information from additional sensors [10]—such as gyrometers or magnetometers—or periodic relocalization from a known accurate position reference [11], [13], such as a GPS signal. Hence, all acceleration-based displacement measurements are prone to significant drift for long-term measurements and lack the reliability to be used for modeling or control purposes.

On the other hand, not all displacement sensing applications require static displacement sensing. Since our tendon vibrator application requires only dynamic displacement sensing, we avoid the drift problem by constraining our measurements to only dynamic displacements. We show that under this constraint, it is possible to achieve real-time displacement measurements sufficiently accurate for modeling and control. This constraint puts a limitation on the applications in which our approach can be used; however, many important applications are still possible, such as frequency domain system identification, active vibration suppression, vibration-based fault monitoring or displacement control of vibrators.

Acceleration-based dynamic displacement measurement approaches were reported in the literature for various purposes. Viswanathan and Baghialakshmi [14] used an underdamped double integration circuit with high-pass filtering to sense the maximum amplitudes demonstrated by systems under mechanical vibration testing. Lewis and Ball [15] developed and tested the accuracy of a similar double integrator system versus displacements recorded by a noncontact transducer. In another study by Ball and Lewis [16], the effect of noise on displacement values obtained via integration of acceleration was quantified, and it was concluded that noise imposes strict limitations on the displacement frequency range that can be accurately sensed. Despite the availability of studies on dynamic displacement sensing via integration, real-time implementation in system identification or control has not been demonstrated. We present methods for and results of a successful implementation in a tendon vibrator in this study.

In our earlier work [17], we built a two-stage critically damped analog integrator, interspaced with high-pass filters for eliminating dc offsets before and after each integration step, similar to the approach in [15]. We concluded that our analog integration circuit was suitable to be used for frequency domain system identification of mechanical systems. In the current study, we extend our earlier work by testing the accuracy of both digital and analog integration methods under varying sampling rates. We conducted frequency domain system identification of a speaker-based tendon vibrator with and without the encoder attachment. Finally, we implemented a feedforward displacement controller and experimentally verified that the vibrator was able to generate sustained amplitude vibrations regardless of the changes in frequency determined by a reference frequency profile.

In Section II, we describe our experimental setup, our analog and digital integration methods, the measure we used for quantifying displacement accuracy, techniques used in the system identification protocol, and feedforward control. In Section III, we present our results on accurate displacement sensing, modeling, and control together with the discussion of their potential applications and limitations. Then, we conclude the paper in Section IV.

II. Methods

A. Experimental Setup

We used a speaker with 8 Ω nominal impedance and 4-in diameter as the actuator of our tendon vibrator [see Fig. 1(a) and (b)]. The most commonly used actuators for tendon vibrators are eccentric-mass motors [18], which do not allow independent control of frequency and amplitude of vibration. Controlling both frequency and amplitude of vibrations requires use of high-bandwidth linear actuators, for which speakers constitute a well-suited and low-cost option.

We used a Logosol pulse-width-modulated (PWM) dc servo amplifier in current mode to drive the speaker. A metal rod rigidly attached to the speaker cone allowed attachment of a high-resolution (1 μm) Renishaw RGH24X incremental linear encoder that served as an accurate reference for displacement measurements. The encoder reader head is attached to the movable element of a linear slide (Del-Tron S2-6 ball slider).

Two accelerometers were used to measure the acceleration of the speaker cone with respect to the speaker base. As depicted in Fig. 1(b), accelerometer 1 (Entran EGAX-F-25, sensitivity 4.045 mV/g, full scale range 25 g) was attached near the center of the speaker cone, while the second accelerometer (Entran EGAXT-F-25, sensitivity 2.860 mV/g, full scale range 25 g) was attached to the speaker base. Acceleration of accelerometer 2 was subtracted from accelerometer 1 in analog signal conditioning, leading to a measurement of differential acceleration, i.e., acceleration of the speaker cone with respect to the base of the speaker. The main advantage that the differential measurement brings is neglecting movements or disturbances that affect the whole setup. Additional advantages of differential measurement are improved noise rejection and robustness against temperature-based drifts in sensitivity and in offset common in accelerometers [19].

For data acquisition (DAQ) and control, we used a host Windows XP PC with Matlab Simulink (by Mathworks Inc.) and QuaRC (by Quanser Inc.) software, connected to a target PC with a Quanser Q4 DAQ board and QNX real-time operating system (RTOS). This host–target configuration with an RTOS on the target ensured reliable DAQ and control up to 20-kHz loop rates.

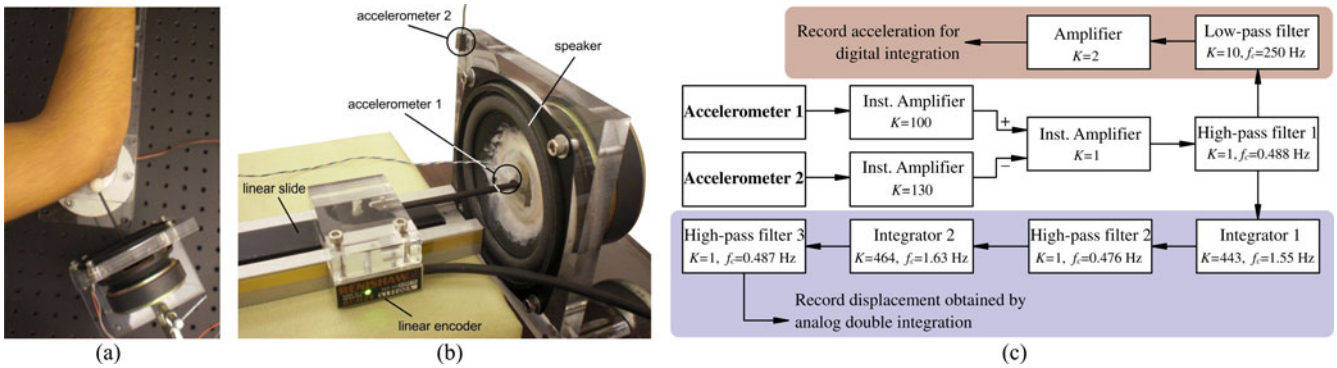

Fig. 1. (a) Speaker-based tendon vibrator in use for applying vibrations on the triceps tendon at the elbow for inducing illusion of elbow flexion. (b) Vibrator with attached accelerometers for differential acceleration measurement and a linear encoder to serve as a reliable displacement measurement reference. We tested the reliability of displacement measurements obtained by double integration in digital and analog domains of differential acceleration in comparison to encoder readings. (c) Block diagram of the analog signal conditioning and double integration circuit. Middle row is common for both integration methods. Top row leads to the acceleration recording by the DAQ board via a low-pass filter for high frequency noise cancelation. Bottom row performs analog double integration and ensures that the dc offset in the signal is always completely removed via high-pass filters before and after each integration step. K represents the gain and f_c represents the cut-off frequency.

B. Signal Conditioning

A block diagram for the complete analog signal conditioning and double integration circuit is given in Fig. 1(c). The middle row in the diagram is the signal conditioning that is common to both analog and digital integration implementations. First, the accelerometer output signals are amplified via Analog Devices AD620 instrumentation amplifiers, the gains of which are adjusted to match the sensitivities of accelerometers. The amplified acceleration signals are then fed into another AD620 with unity gain in differential configuration where acceleration 1 is subtracted from acceleration 2. Before splitting into digital and analog integration paths, the dc component in the differential acceleration is removed by a first-order unity gain high-pass filter with 0.488-Hz cut-off frequency. All high-pass and low-pass filters in the analog signal conditioning circuit use LF412 operational amplifiers.

C. Analog Double Integration

The analog integration circuit includes first-order high-pass filters with a cut-off frequency close to 0.5 Hz and first-order low-pass filters with a cut-off frequency close to 1.5 Hz, as depicted in the bottom highlighted row in Fig. 1(c). The circuit diagrams for this double integrator and its transfer function can be found in our earlier work [17]. High-pass filters are used to remove dc offsets in the signals that lead to significant drift when integrated. Low-pass filters act as integrators for the frequency range above their cut-off frequency of 1.5 Hz. Cascading these high-pass and low-pass filters leads to a two-stage double integrator that ignores static movements (below 0.5 Hz), but allows for measurement of dynamic (above 1.5 Hz) displacement from only differential acceleration measurements.

D. Digital Double Integration

The digital integration path, which can be followed to the highlighted top row in Fig. 1(c), includes a low-pass filter with a gain of 10 in the pass-band and a cut-off frequency of 250 Hz, chosen to ensure that high-frequency noise primarily attributable to the PWM servo amplifier is removed. Another amplifier stage with a gain of 2 ensures proper use of the analog input channel resolution.

For numerical integration, the trapezoidal integration method is used. The advantages of digital integration versus analog integration include better noise immunity, easier implementation, and modifiability. On the other hand, digital integration still requires analog signal conditioning and high-loop rates for real-time implementation.

Since the accuracy of the amplitudes of the signals is of critical importance for integration, we used discrete Butterworth high-pass filters (HPF) for removing dc offsets in signals, due to their ideal flat response in the passband. We tested Butterworth filters with varying orders, cut-off frequencies, and sampling rates. For all digital double integrator algorithms that we have tested, we followed the same consecutive high-pass filtering (three stages) and integration (two stages) cascaded structure used for the analog double integrator. The high-pass filters that we have tested included those with order $n = 1$ with cut-off frequencies $f_c = 0.25$ and 0.5 Hz, and those with order $n = 2$ with cut-off frequencies $f_c = 0.25, 0.5, 1$, and 1.5 Hz. Our extensive testing with the vibrator using swept sine waves as well as constant frequency sinusoid driving signals indicated that the most accurate double integration in terms of both amplitude and phase was obtained by using the filter with order $n = 2$ and cut-off frequency $f_c = 1$ Hz. This specific filter was used for all digital integration results reported in this paper. Lower order ($n = 1$) high-pass filters caused low-frequency ($<$0.5 Hz) drifts that significantly distorted the displacement measurements while higher cut-off frequencies ($>$1.5 Hz) or filter order ($>$3) suffered from greater errors in phase.

In order to quantify the accuracy of different integration methods in extracting dynamic displacement data based on acceleration, we calculated the normalized (percent) root-mean-squared (RMS) error

$$\text{Percent error}(x_{\text{int}}, x_{\text{enc}}) = 100\frac{\|x_{\text{int}} - x_{\text{enc}}\|}{\|x_{\text{enc}}\|}. \quad (1)$$

Here, x_{int} is the array of displacement values obtained via integration, and x_{enc} is the array of displacement values recorded by the encoder. It should be noted that this measure of accuracy penalizes errors in both amplitude and phase. Penalization of both types of errors is in fact desired in our application, since accurate sensing of displacement with accurate timing is required. Hence, this accuracy measure serves as an appropriate measure to quantify the accuracy of dynamic displacement sensing via double integration.

E. System Identification

We used frequency domain system identification techniques to obtain a mechanical plant model for the speaker. The input of the plant was voltage applied via an analog output channel of the DAQ board, which

corresponded to a proportional current applied to the speaker coil. The output of the plant was displacement, measured simultaneously by the encoder and by double integration of differential acceleration.

Among multiple excitation signal options for system identification, we opted for a Schroeder multisine. A Schroeder multisine excitation signal has the favorable property of having a flat autospectrum along the frequency range of interest, allowing injection of evenly distributed energy into the system within the bandwidth [20]. As our excitation signal, we generated a 60-s Schroeder multisine with a bandwidth of 1–100 Hz at a sampling rate of 20 kHz.

With the output of the system $y(t)$ in response to the input $u(t)$ at hand, the so-called H_1 frequency response function (FRF) can be calculated for the system by

$$H_1(f) = \frac{P_{UY}(f)}{P_{UU}(f)} = \frac{Y(f)}{U(f)}\frac{U^*(f)}{U^*(f)}. \quad (2)$$

Here, f represents frequency, $P_{UY}(f)$ and $P_{UU}(f)$ are cross- and auto-power spectral densities, respectively, calculated based on the power spectral densities of the input and the output, $U(f)$ and $Y(f)$.

In developing the H_1 FRF for the speaker, we made use of windowing and averaging methods in order to further decrease the effects of noise in measurements. We used a Hanning window with 2^{15} window length and 75% overlap between consecutive data segments, resulting in a frequency resolution of approximately 0.610 Hz in the estimated FRFs. The experimental FRFs constituted our nonparametric models for the speaker. To obtain a parametric model, we assumed a continuous second-order transfer function (TF) structure

$$G(s) = \frac{K\omega_n^2}{s^2 + 2\zeta\omega_n s + \omega_n^2}. \quad (3)$$

We identified the parameters of this model via a least-squares fitting method, and used a higher weight (with a ratio of 6:1) for the frequency components between 10 and 100 Hz in estimation, since this interval constituted our frequency range of interest and major dynamics of the system (resonance) took place in this interval in all cases. In order to verify the accuracy of the obtained model, we developed a feedforward displacement controller and tested the performance of the controlled system experimentally in tracking a reference signal.

III. Results and Discussion

A. Accuracy of Displacement Measurements via Analog and Digital Double Integration

Table I provides a summary of percent error values between the encoder readings and displacement values obtained by analog integration and trapezoidal integration at varying sampling rates. The data used for this table are obtained when driving the vibrator with a 1–50 Hz swept sine signal lasting 30 s. The first 3 s of each dataset are ignored due to high error for low frequencies outside the sensing range of integration methods. In interpreting the error values reported in this table, remember that the percent error measure highly penalizes errors due to phase, and in all cases considered here, minor phase difference is the major source of error. The actual measurement curves in Fig. 2 give a qualitative sense of displacement measurement accuracy via integration in terms of amplitude and phase. Note that the percent error values for digital and analog integration for the equivalent conditions in Fig. 2 are around 30%, as listed on the first row of Table I.

A comparison between the discrete trapezoidal integration method and the analog integration method reveals that their accuracies are very close for sampling rates between 100–20 000 Hz. Trapezoidal integration demonstrates a lower percent error value than analog integration for most of the cases within this frequency range, mostly due to slightly better phase accuracy. At sampling rates below 100 Hz, only the analog integration method can be used reliably.

TABLE I
Accuracy of Digital and Analog Integration Methods in Extracting Displacement Data from Acceleration at Various Sampling Rates

	Percent error of first data set wrt second	
Sampling Rate (Hz)	$x_{analog\ int}$, x_{enc}	$x_{dig\ trap\ int}$, x_{enc}
20,000	33.8	29.7
1,000	33.7	29.4
500	33.8	29.6
200	33.6	29.2
100	33.7	31.5
66.7	34.0	75.9
50	34.1	91.0

Percent error values (See Eq. 1) are listed for given data pairs, for a 30-sec long swept sine wave excitation from 1 Hz To 50 Hz.

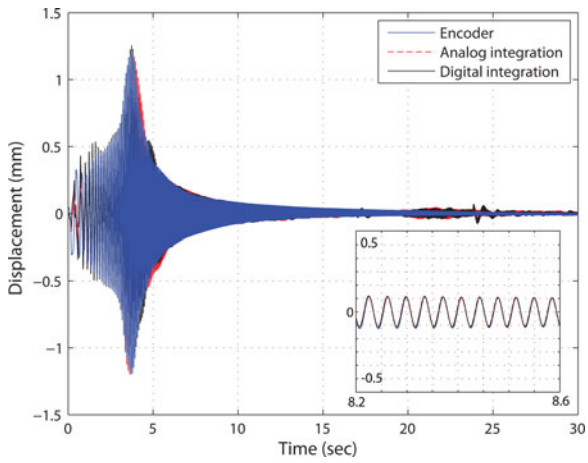

Fig. 2. Displacement values obtained via both digital and analog double integration are highly accurate. Inset provides a zoom in on to the data between 8.2–8.6 s, where three signals are indistinguishable.

We observed that displacement measurements via digital integration were always less noisy than those obtained via analog integration. Another positive aspect of digital integration was higher accuracy at high sampling rates, as compared to analog integration. On the other hand, digital integration methods were less accurate in sensing very small displacements as can be observed in Fig. 2 near $t = 24$ s. This deviation is due to acceleration measurements becoming inaccurate with the coarsening of quantization resolution during small displacements. This observation indicates the suitability of the analog integration method in applications, where displacement amplitudes show high variability, requiring accurate measurement of both large and small displacements. Nevertheless, both integration methods presented here can be used to accurately measure dynamic displacement via only acceleration measurements, and these measurements are sufficiently reliable to be used in frequency domain system identification and control, as discussed in the next section.

B. System Identification and Control

1) Model of the Tendon Vibrator with Encoder Attachment: The system identification protocol in Section II-E was followed with the encoder attached to the vibrator, allowing a comparison of models obtained with encoder recordings and those obtained with displacements measured by proposed analog and digital integration methods. Fig. 3

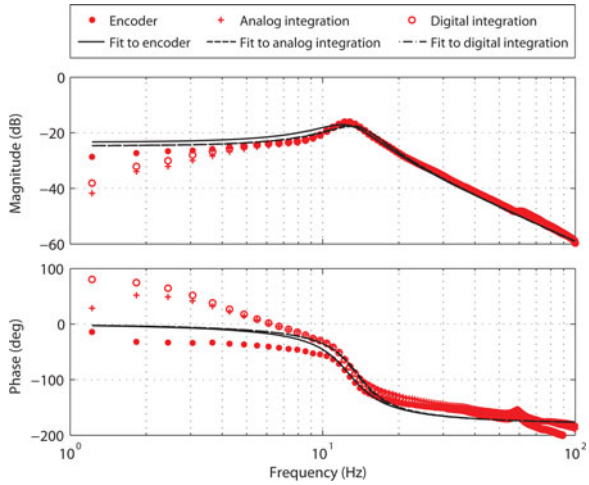

Fig. 3. Experimental FRFs for the tendon vibrator with the encoder attachment obtained via displacements measured by encoder, analog integration, and digital integration. These FRFs and TF fits to the FRFs show that identified models using different displacement measurement methods match closely, especially in the frequency range of 10–100 Hz. This agreement enables obtaining accurate models solely based on integrated acceleration measurements.

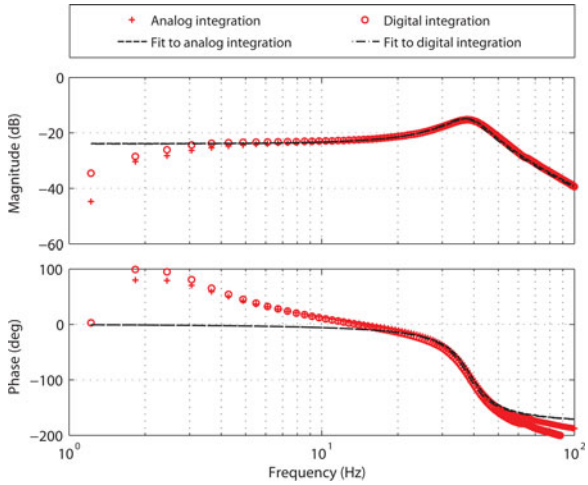

Fig. 4. Experimental FRFs for the tendon vibrator after the encoder was detached, obtained via displacements measured by analog integration and digital integration. Comparing these FRFs and TF fits with those in Fig. 3 demonstrates that the encoder attachment vastly changes the dynamics of the vibrator, by pushing the resonance frequency from around 38 Hz to around 13 Hz. Conducting the system identification using only accelerometers enables undisturbed estimation of the plant dynamics and does not deteriorate the system bandwidth.

TABLE II
ESTIMATED MODEL PARAMETERS FOR THE MODEL STRUCTURE GIVEN IN (3) USING DISPLACEMENT MEASUREMENTS BY ENCODER, ANALOG INTEGRATION AND DIGITAL INTEGRATION

Displacement measured by	Estimated model parameter values		
	K (mm/V)	ζ (no units)	ω_n (rad/s)
encoder	−0.6789	0.2499	80.09
analog integration	−0.5820	0.2287	86.47
digital integration	−0.5842	0.2213	85.61

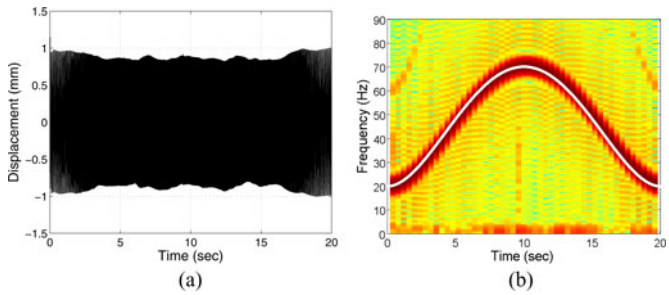

Fig. 5. (a) Sustained ± 1 mm displacement profile as measured by the analog integrator for the desired vibration profile given by the white curve in (b). (b) Agreement between the time–frequency plot of the displacement profile given in the background and overlaid desired vibration profile (white curve) shows the accuracy in instantaneous frequency.

shows the experimental FRFs and the TF fits obtained for the vibrator using displacement measurements from the encoder, from analog integration and from digital integration. The three FRFs are in good agreement for the frequency range 10–100 Hz. The deviations within the 1–10 Hz range are consequences of the accuracy of the acceleration based dynamic displacement measurements. The TF fits in Fig. 3 that focus on the frequency range of 10–100 Hz show that the models obtained based on both integration methods match very closely the model based on encoder measurements. The estimated numerical values of the parameters for the assumed model structure in (3) are summarized in Table II for all three TF fits in Fig. 3. The results summarized in this table justify the use of displacement measurements via both integration methods for accurate system identification of the vibrator. Based on this result, we removed the encoder from the system and reran our system identification protocol.

2) Model of the Tendon Vibrator without Encoder Attachment: The FRFs and TF fits with estimated parameters when the encoder was detached from the vibrator are given in Fig. 4. The TF obtained in Fig. 4 by using the digital integration method was given by

$$G(s) = \frac{-3560}{s^2 + 83.99s + 56246}. \quad (4)$$

By comparing the TFs in Fig. 3 with those in Fig. 4, it is apparent that attaching the encoder with its nonnegligible mass to the speaker to measure displacement vastly changes the dynamics of the system, moving the resonance from 38 to 13 Hz and decreasing the system bandwidth. By using the differential acceleration measurements and double integration, we can accurately sense the displacement of the vibrator and obtain an accurate and undisturbed model of it. Hence, it is advisable to use the reported sensing and modeling methods when it is critical to model the dynamics of a system with minimal interference, or to take dynamic displacement measurements from a plant with minimal disturbance to the original operating conditions of the plant. Noncontact laser displacement sensors provide this capability, but are significantly more expensive than accelerometers.

3) Feedforward Control of the Tendon Vibrator and Model Validation: In order to evaluate the validity of the obtained model (4), we tested the performance of the vibrator in tracking a reference displacement profile under feedforward control. The controller scales the control effort online based on the desired instantaneous frequency effectively by multiplying it by $1/|G(j\omega)|$. For the reference frequency profile given in Fig. 5(b), the amplitude of the vibrations are successfully sustained at ± 1 mm as can be observed in Fig. 5(a). Fig. 5(b) also reports the accuracy of the frequency tracking as given by the time–frequency plot of the vibrations in Fig. 5(a) based on short-time Fourier transforms.

The successful feedforward control implementation demonstrates the effectiveness of using differential acceleration measurements and

proposed double integration methods for dynamic displacement sensing, system identification, and control of our tendon vibrator. Although we do not report explicit results for velocity sensing, our results extend to accurate velocity sensing and control, since it is a simpler problem and actually an intermediate step in our algorithms.

As long as the modeling or operation frequency range of interest for the plant is lower bounded, i.e., only dynamic displacements are of interest, the accelerometer-based sensing and identification method that we propose can be applied. Potential applications include frequency domain system identification of mechanical systems, civil engineering systems [21] or of human impedance in haptic interactions [22]: feedback or feedforward control scenarios that involve dominantly dynamic displacements, such as active vibration suppression [23], shaker or vibrator displacement control and active speaker control. Also, having velocity and displacement information in addition to acceleration can improve vibration-based fault monitoring and detection methods [24].

The tendon vibrator that we have developed demonstrates the capability of applying vibrations with sustained amplitudes and with accurate prescribed frequency profiles. This novel capability will facilitate future research to determine the effects of various vibration characteristics on the consistency, controllability, and perception of vibration-induced movement illusions for smart prosthetics, among other potential applications.

IV. Conclusion

This study presented results from successful implementation of system identification and feedforward control based on only acceleration measurements and double integration methods for displacement sensing in a speaker-based tendon vibrator. We tested both digital and analog integration methods and quantified their displacement sensing accuracy under varying sampling rates. Dynamic displacement sensing and control based on differential acceleration measurements have potential applications in active vibration suppression and vibration-based fault monitoring, among others. This method also provides a solution to the problem of system identification with minimal distortion to original plant dynamics in a cost effective way as compared to currently available solutions such as laser displacement sensors.

References

[1] F. Albert, M. Bergenheim, E. Ribot-Ciscar, and J. P. Roll, "The Ia afferent feedback of a given movement evokes the illusion of the same movement when returned to the subject via muscle tendon vibration," *Exp. Brain Res.*, vol. 172, no. 2, pp. 163–174, 2006.

[2] G. M. Goodwin, D. I. McCloskey, and P. B. Matthews, "The contribution of muscle afferents to kinaesthesia shown by vibration induced illusions of movement and by the effects of paralysing joint afferents," *Brain, A J. Neurol.*, vol. 95, no. 4, pp. 705–748, 1972.

[3] J. R. Lackner, "Some proprioceptive influences on the perceptual representation of body shape and orientation," *Brain*, vol. 111, no. 2, pp. 281–297, 1988.

[4] E. Naito, H. H. Ehrsson, S. Geyer, K. Zilles, and P. E. Roland, "Illusory arm movements activate cortical motor areas: a positron emission tomography study," *J. Neurosci.*, vol. 19, no. 14, pp. 6134–6144, 1999.

[5] J. P. Roll and J. P. Vedel, "Kinaesthetic role of muscle afferents in man, studied by tendon vibration and microneurography," *Exp. Brain Res.*, vol. 47, no. 2, pp. 177–190, 1982.

[6] S. Miyazaki, "Long-term unrestrained measurement of stride length and walking velocity utilizing a piezoelectric gyroscope," *IEEE Trans. Biomed. Eng.*, vol. 44, no. 8, pp. 753–759, Aug. 1997.

[7] R. E. Mayagoitia, A. V. Nene, and P. H. Veltink, "Accelerometer and rate gyroscope measurement of kinematics: An inexpensive alternative to optical motion analysis systems," *J. Biomech.*, vol. 35, no. 4, pp. 537–542, 2002.

[8] T. Pfau, T. H. Witte, and A. M. Wilson, "A method for deriving displacement data during cyclical movement using an inertial sensor," *J. Exp. Biol.*, vol. 208, no. 13, pp. 2503–2514, 2005.

[9] J. Borenstein, L. Ojeda, and S. Kwanmuang, "Heuristic reduction of gyro drift for personnel tracking systems," *J. Navigat.*, vol. 62, pp. 41–58, 2008.

[10] J. K. Lee and E. J. Park, "Minimum-order Kalman filter with vector selector for accurate estimation of human body orientation," *IEEE Trans. Robot.*, vol. 25, no. 5, pp. 1196–1201, Oct. 2009.

[11] K. Parsa, T. A. Lasky, and B. Ravani, "Design and implementation of a mechatronic, all-accelerometer inertial measurement unit," *IEEE/ASME Trans. Mechatronics*, vol. 12, no. 6, pp. 640–650, Dec. 2007.

[12] G. Pang and H. Liu, "Evaluation of a low-cost mems accelerometer for distance measurement," *J. Intell. Robot. Syst.*, vol. 30, no. 3, pp. 249–265, 2001.

[13] S. P. Kwakkel, "Human lower limb kinematics using gps/ins" Master's thesis, Dept. Geomatics Eng., University of Calgary, Alberta, Canada, 2009.

[14] R. Viswanathan and S. Baghialakshmi, "A direct acceleration and displacement meter using op-amps.," *Indian J. Tech.*, vol. 12, pp. 536–539, 1974.

[15] C. P. Lewis and R. Ball, "An instrument for the measurement of structural vibrations," *J. Strain Anal. Eng. Design*, vol. 14, no. 4, pp. 165–169, 1979.

[16] R. Ball and C. P. Lewis, "Effect of noise when deriving signals from accelerometers," *Meas. Control*, vol. 15, pp. 59–61, 1982.

[17] H. B. Gilbert, O. Celik, and M. K. O'Malley, "Long-term double integration of acceleration for position sensing and frequency domain system identification," in *Proc. IEEE/ASME Int. Conf. Adv. Intell. Mechatronics*, 2010, pp. 453–458.

[18] O. Celik, M. K. O'Malley, R. B. Gillespie, P. A. Shewokis, and J. L. Contreras-Vidal, "Compact and low-cost tendon vibrator for inducing proprioceptive illusions," in *Proc. IEEE World Haptics Conf.*, 2009, pp. 623–624.

[19] W. T. Ang, P. K. Khosla, and C. N. Riviere, "Design of all-accelerometer inertial measurement unit for tremor sensing in hand-held microsurgical instrument," in *Proc. IEEE Int. Conf. Robot. Autom.*, 2003, pp. 1781–1786.

[20] R. Pintelon and J. Schoukens, *System Identification: A Frequency Domain Approach*. New York: IEEE Press, 2001.

[21] G. Jin, M. K. Sain, and B. F. Spencer Jr., "Frequency domain system identification for controlled civil engineering structures," *IEEE Trans. Control Syst. Technol.*, vol. 13, no. 6, pp. 1055–1062, Nov. 2005.

[22] R. Balasubramanian, R. Howe, and Y. Matsuoka, "Task performance is prioritized over energy reduction," *IEEE Trans. Biomed. Eng.*, vol. 56, no. 5, pp. 1310–1317, 2008.

[23] A. J. Den Hamer, G. Z. Angelis, and N. B. Roozen, "Broad-band active vibration suppression using PPF focused on industrial application," *IEEE/ASME Trans. Mechatronics*, vol. 10, no. 2, pp. 146–153, Apr. 2005.

[24] W. Wang and O. A. Jianu, "A smart sensing unit for vibration measurement and monitoring," *IEEE/ASME Trans. Mechatronics*, vol. 15, no. 1, pp. 70–78, Feb. 2010.